CHINESE JOURNAL OF PHYSICS VOL. 53, NO. 7 December 2015

Molecular Dynamics Study of Uniaxial Deformation in Perfect and Defective Aluminum

Bin Tang[1] and Rong Yang[2,*]

[1] *Institute of Finance & Trade, Chongqing City Management College, Chongqing 401331, PR China*
[2] *College of Materials Science and Engineering, Chongqing Jiaotong University, Chongqing 400074, PR China*

(Received December 15, 2014; Revised September 19, 2015)

In materials, strength is usually controlled by the occurrence of grain boundaries, dislocations, voids, and other microstructural defects. molecular dynamics (MD) simulations with the embedded atom method potential have been employed to investigate the uniaxial tension and compression of single crystal aluminum with and without defects. In this paper, defect refers to a void or grain boundary. For perfect crystal aluminum, the ideal strengths and stress-strain curves obtained from the MD simulations agree well with those obtained by first principles calculations. The strength and ductility of Al decrease with the occurrence of void and grain boundaries. The effect of void size on the uniaxial stress-strain relations is investigated. Also, dislocation nucleation and emission from the void free surface are observed. In order to study the effect of a grain boundary, we generate a symmetric tilt grain boundary $\Sigma5(310)$ and strain is imposed perpendicular to the boundary interface. We can clearly see that fracture starts in the grain boundary. The observed defect pattern is expected to provide some helpful insights into the damage mechanism of ductile materials at the microscale. The effects of temperature, strain rate, and crystalline direction on the ideal strength are also discussed.

DOI: 10.6122/CJP.20150928A PACS numbers: 62.20.-X, 62.20.D-, 62.20.F-

I. INTRODUCTION

Aluminum has been widely applied in the microelectronic, automotive, and aerospace industries, because it is one of the lightweight structural materials with good mechanical properties and castability [1–3]. One fundamental measure of the mechanical strength of a material is its ideal strength. The ideal strength of a material is the first maximum stress in the stress-strain curve when the material is deformed. When the stress is increased to the ideal strength in deformation, a perfect crystal becomes mechanically unstable [4, 5]. So if the perfect crystal is deformed beyond the elastic limit, plastic deformation will be allowed. The ideal strength is the upper limit of the strength of a real crystal, so it is very meaningful to study the ideal strength. We will discuss uniaxial tension and uniaxial compression in this paper.

Both molecular dynamics (MD) simulation and first-principles calculation can be employed to study uniaxial deformations. Molecular dynamics with various empirical po-

*Electronic address: cqyr88@126.com

tentials has been applied to simulate a uniaxial deformation by numerous authors [6–9]. The simulated systems are not only bulk materials but also are expanded to micrometer or nanometer sized materials. The ideal strength is one of the few mechanical properties that can be calculated from first principles. A number of first-principles calculations of the ideal strength [10–12] have been carried out. The results generated by MD strongly depends on the adopted potential, so the results of the MD simulations which depend on the quality of the semi-empirical potential are not reliable as first-principles calculations, but MD simulations can provide important insights into the atomic mechanisms of the kinetic processes occurring during deformation. In this paper we combine these two methods to investigate the uniaxial deformation in aluminum.

Previous studies [6–8, 11, 12] have focused mainly on the perfect single crystal without any defect. However experimental samples always have defects, such as dislocation, voids, and grain boundaries. It follows that the experimental estimates of ideal strength are far below the values predicted by the theoretical calculations. The aim of this paper is to carry out MD simulations of uniaxial deformation in aluminum with defects (void or grain boundaries), in order to explore the effect of defects on the ideal strength, and the underling damage mechanism of ductile materials. For perfect crystal aluminum, we also use first principles to calculate the ideal strength for checking and comparing. The effects of temperature, strain rate, and crystalline direction on the ideal strength and critical strain are also analyzed in this study.

The paper is organized as follows. Computational methods and details are presented in Section II. We give the results and discussions in Section III. Finally, the conclusions are summarized in Section IV.

II. COMPUTATIONAL METHOD AND DETAIL

II-1. MD simulations

The MD simulations strongly depend on the interaction potential among the constituting atoms. Here we adopt the embedded atom method (EAM) [13] potential published by Mishin in 1999 [14], because the potential accurately reproduces the elastic constants, the vacancy formation and migration energies, the stacking fault energies, and the surface energies. The following MD simulations are performed using the large-scale atomic/molecular massively parallel simulator (LAMMPS) program developed by Plimpton *et al.* (1995) [15]. The ATOMEYE software developed by Li [16] is used to visualize the atomistic configuration.

If we want to study the uniaxial deformation in the <100> direction using MD simulations, we first generate a $20 \times 20 \times 20$ primitive FCC cell with <100> orientation in the x direction, <010> orientation in the y direction and <001> orientation in the z direction, so the simulated system contains 32000 Al atoms. I choose so large a simulation cell size in order not to influence the dislocation nucleation mechanism. Periodic boundaries are applied in all directions. To simulate the uniaxial deformation, the simulation cell is relaxed for 70 ps (20,000 time steps) at zero force to minimize the potential energy as a

first step. Then the simulation cell is deformed in the x direction at a strain rate of 10^{10} s^{-1}, while the lateral boundaries are controlled using the NPT ensembles to zero pressure.

Before the simulation of uniaxial deformation, we need to check the quality of the adopted potential. First the lattice parameter is computed via the cohesive energy. Our calculated value is 4.050 Å, it is in good agreement with the experimental value of 4.045 Å [17]. Then the elastic constants, which can well describe the mechanical properties of materials in elastic deformation, have been computed. There are three independent elastic constants c_{11}, c_{12}, and c_{44} for cubic symmetry. The results are listed in Table I. Our calculated elastic constants also agree well with the experimental data [18], so the following simulations will take the EAM potential.

TABLE I: Calculated and experimental elastic constants of Al. Experimental elastic constants are from Ref. [18].

Al	EAM	EXPT	%Error
C_{11}	113.8	108.0	5.3%
C_{12}	61.6	62.2	−0.96%
C_{44}	31.6	28.4	11.3%

II-2. First-principles calculations

In this work, the first principles calculations based on density functional theory (DFT) are performed using the VASP software package [19]. During our calculations, the generalized gradient approximation (GGA) Perdew-Wang 91 exchange-correlation functional [20] and the projector augmented-wave (PAW) pseudopotential are used [21]. In order to achieve the convergence, the Monkhorst-Pack (MP) [22] k-point grid is set as $24 \times 24 \times 24$ and the plane-wave cutoff energy is set to 350 ev.

Calculations of the ideal strength using the VASP code employ the following method. First we construct a unit cell which contains 4 Al atoms. The incremental strain is imposed on the direction of the applied stress. At each step the structure must be fully relaxed such that all of the components of the stress tensor orthogonal to the direction are less than 0.1 GPa [11].

III. RESULTS AND DISCUSSIONS

III-1. Perfect single crystal Al

III-1-1. Ideal strength and stress-strain curve

We impose a tensile strain and a compressed strain on crystal Al. The strain is imposed in the high-symmetry direction <100>. The essential results are summarized in Table II. First principles calculations in this work are run at 0 K, whereas the MD simulations are performed at 10 K. We don't perform the MD simulation at 0 K, because

the NPT ensembles cannot be controlled at 0 K.

TABLE II: Ideal tensile strength and ideal compressed strength.

Ideal strength (GPa)	DFT	EAM
<100> tension	11.33	11.10
<100> compression	8.32	8.30

We note that our first-principles result of the ideal tensile strength (11.33 GPa) is close to the work of Clatterbuck *et al.* (2003) [11]. Clatterbuck *et al.* [11] obtained 12.92 GPa using the local density approximation (LDA). It is known that the LDA produces strengths 10%–20% higher than the GGA. According to Table II, the MD simulation results at 10 K are close to the values obtained by first-principles calculations. Because our first-principles calculations compared with the work of Clatterbuck *et al.* [11] are reliable, we expect the MD simulations in this work are also reliable. Besides, we can see that the ideal compressed strength is smaller than the ideal tensile strength, so compression can more easily make the crystal mechanically unstable than tension for Al.

For brevity, we only present the stress-strain curve of <100> uniaxial compression (see Fig. 1). The curve terminates near the peak stress. In general, two methods give a similar curve trend. First the stress rises almost linearly to the maximum with the strain, the peak stress in the stress-strain curve is the ideal strength discussed previously, the strain corresponding to the ideal strength is usually called the critical strain. Then after the peak point in the stress-strain curve, the stress decreases, this means that the deformation exceeds the elastic limit and plastic deformation occurs.

In order to understand why the stress drops beyond the critical strain, we use the ATOMEYE software to visualize the deformation process under <100> uniaxial compression. The centro-symmetry parameter defined by Kelchner *et al.* [23] is employed to illustrate the deformation. The parameter is given by $P = \sum_i |\mathrm{R}_i + \mathrm{R}_{i+6}|^2$, where R_i and are R_{i+6} are the vectors corresponding to the six pairs of opposite nearest neighbors in the FCC lattice [23]. For an atom on a perfect lattice, the centro-symmetry parameter will be 0. When a local defect (a dislocation or stacking fault) exists, the symmetry is broken, so the parameter will increase. An atom at a surface will have a large positive parameter. For single crystal Al, $0.5 < P < 3$ corresponds to a partial dislocation, $3 < P < 16$ corresponds to stacking faults and $P > 16$ corresponds to surface atoms. To clearly see a defect, we make the perfect atoms invisible. Fig. 2(d), Fig. 2(e), and Fig. 2(f) only show the atoms in a non-centrosymmetric environment.

The critical strain corresponding to the ideal strength is 0.12 at 10 K. We select the images at 0.12, 0.13, 0.14 strain, as shown in Fig. 2. At strain 0.12, the centro-symmetry is nearly 0 everywhere, the atoms are still in a perfect lattice (see Fig. 2(a) and 2(d)). We can see nucleated dislocations beyond the critical strain (see Fig. 2(e) and Fig 2(f)), it indicates that plastic deformation occurs, and it can explain why the stress decreases beyond the critical strain (see Fig. 1). So MD simulations can provide important insights

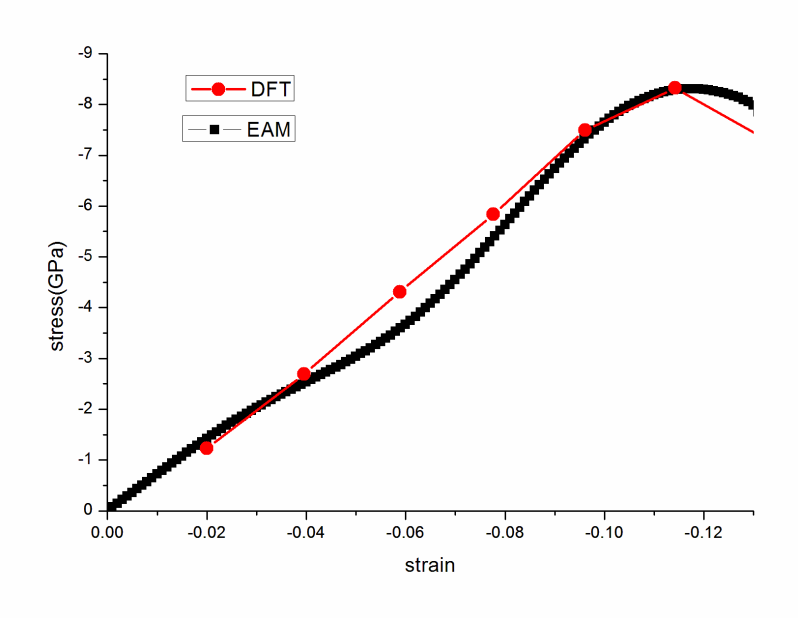

FIG. 1: (Color online) Stress-strain curves for <100> uniaxial compression.

into the atomic mechanisms of kinetic processes occurring during deformation. Whereas the first-principles method only performs the deformation in a unit cell, it studies the nature of deformation from the atomic microstructure and intrinsic chemical bonding. We can see the difference between the two methods (MD simulations and first-principles calculations) from Fig. 3. When the strain is imposed on the x direction, the basis vector a changes identically with the strain using first-principles calculations and MD simulations (see Fig. 3a). The basis vectors b and c change identically with the strain in first-principles calculations. But in MD simulations the basis vectors b and c change identically with the strain only before the critical strain 0.12, as shown in Fig. 3b. After the critical strain, the development of the basis vector c obtained from the MD simulation is smaller than that obtained by first-principles, the development of the basis vector b for the MD simulation and first principles is similar. In MD simulations, the difference in the development of the lattice parameters b and c means that slips take place after critical strain.

III-1-2. Temperature effect

In this section, the influence of temperature on the tensile deformation of a perfect single aluminum crystal is considered. Fig. 4 shows the curves of ideal strength and critical strain with temperature. It clearly demonstrates that thermal effects play an important role in the tensile deformation of single crystal aluminum. It is interesting that from the temperatures of 100 K to 400 K, the ideal strength decreases approximately linearly with increasing temperature. This is because thermal fluctuations at elevated temperature can assist structural instability. The strain corresponding to the ideal strength (i.e., the

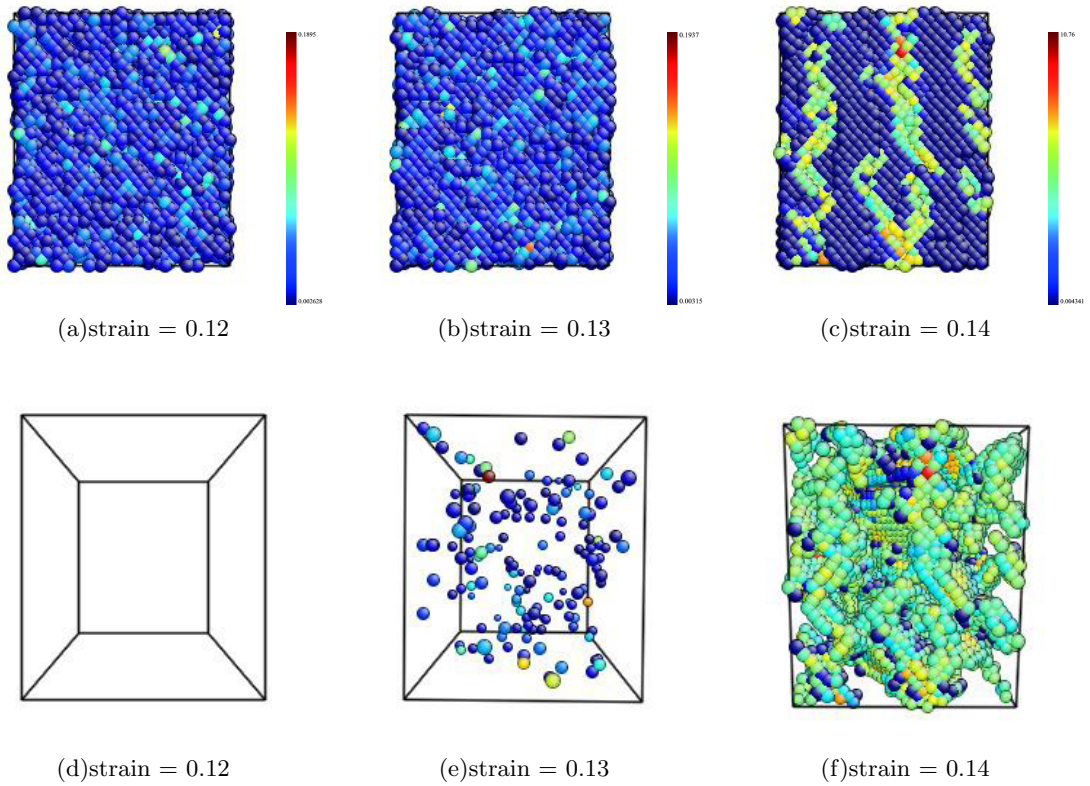

(a)strain = 0.12 (b)strain = 0.13 (c)strain = 0.14

(d)strain = 0.12 (e)strain = 0.13 (f)strain = 0.14

FIG. 2: (Color online) Deformed atomistic configurations under <100> uniaxial compression at 10 K. The crystal orientation is [100]-[010]-[001]. Atoms are color-coded according to their central symmetry parameter P in the range between (a) 0 and 0.1895, (b) 0 and 0.1937, (c) 0 and 10.76.

critical strain) also decreases with increasing temperature, it also means that increasing temperature can more easily make the crystal mechanically unstable.

III-1-3. Strain rate effect

In order to investigate the effect of the strain rate on the tensile deformation, five different strain rates, i.e., 5×10^{10} s^{-1}, 10^{10} s^{-1}, 5×10^{9} s^{-1}, 10^{9} s^{-1}, and 10^{8} s^{-1} are considered. Fig. 5 shows the stress-strain curves for different strain rates at 300 K. We can find that as the strain rate increases from 10^{8} s^{-1} to 5×10^{10} s^{-1}, the peak strength increases from 7.39 GPa to 8.59 GPa, while the initial slope of the stress-strain curve is insensitive to the strain rate. The strain at the peak also increases with increasing strain rate.

III-1-4. Crystalline direction effect

The ideal strength is sensitive to the deformation direction. To study the effect of different orientations on the tensile deformation, we construct a regular FCC lattice with

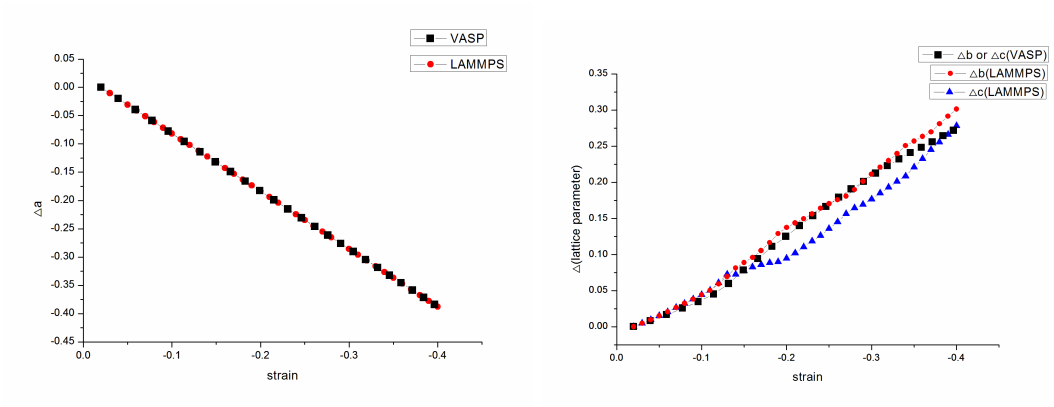

(a) (b)

FIG. 3: (Color online) The increments of the lattice parameters a, b, and c ($\Delta x = (x - x_0)/x_0$, $x = a, b, c$) with the strain for <100> uniaxial compression. When the strain is 0, the lattice parameter is x_0 ($x = a, b, c$).

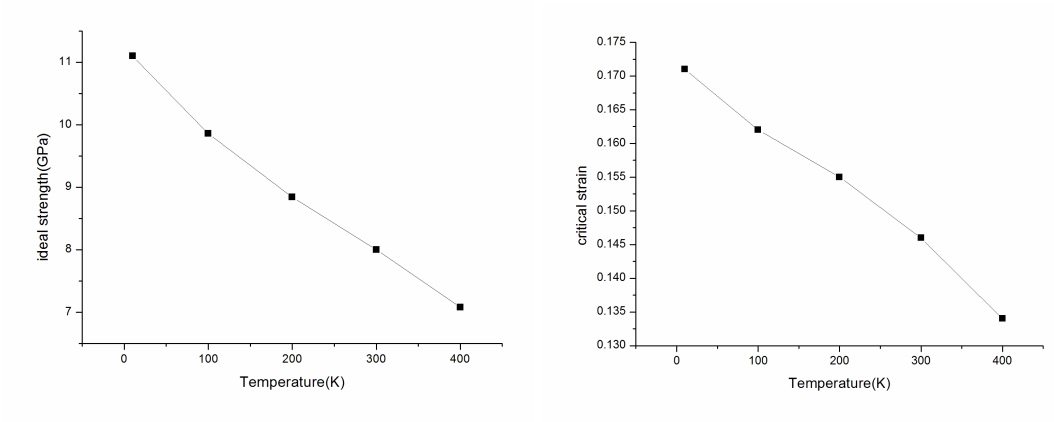

(a) (b)

FIG. 4: (a) Curves of ideal strength as a function of temperature. (b) Curves of ideal critical strain as a function of temperature under <100> uniaxial tension.

initial surface orientations of [001], [1$\bar{1}$0], [110] in the x, y, and z directions, respectively. Uniaxial tension is performed along the z-direction. The <110> orientation is also of great interest for FCC materials by noting that <110> is the most closely packed direction. The stress-strain curve in the <110> direction is shown in Fig. 6, compared with the <100> tensile curve. The values of the peak stresses under the <100> and <110> tensions at 300 K are 8.00 GPa and 2.67 GPa, respectively. It is obvious that at room temperature the tensile strength has reduced by about 67%. So the weak direction for a tensile deformation is the <110> direction for aluminum.

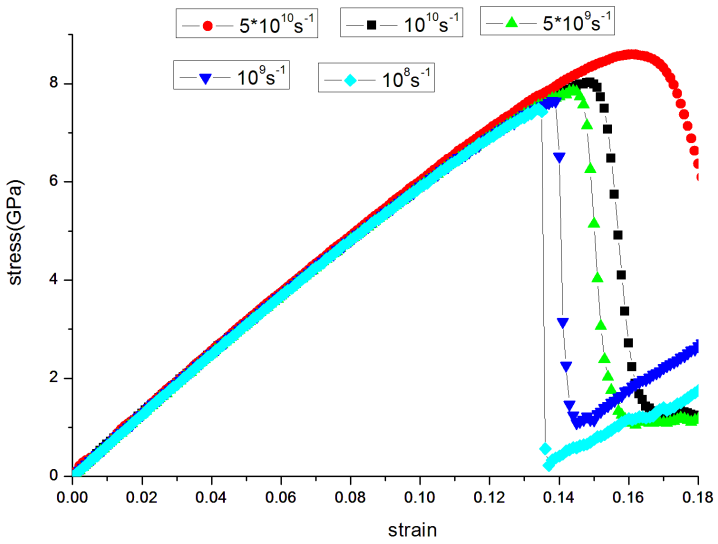

FIG. 5: (Color online) Stress-strain curves of tensile deformation at different loading rates at 300 K. The loading is applied along the [100] direction.

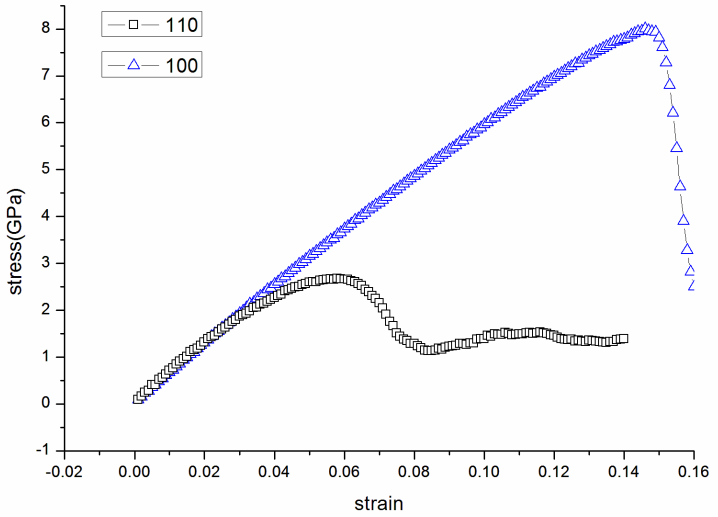

FIG. 6: (Color online) Stress-strain curves of tensile deformation at different crystalline directions at 300 K.

III-2. Single crystal Al with defect

III-2-1. Void effect

For ductile metals (e.g., Al), nucleation, growth, and coalescence of voids eventually leads to the fracture of materials [12]. In order to investigate the void effect in aluminum subjected to uniaxial tension, we construct a $20\times20\times20$ simulated system with a cylindrical hole, which is shown in Fig. 8(a). And the strain is applied in the <100> direction.

First we consider the effect of void volume on the ideal strength. Here two cases are discussed. Case-1: the void height is systematically varied, while the void radius is kept to be a constant 1 Å. When the height is increased from 1 Å to 4 Å and 9 Å, the void volume is correspondingly increased from V to 4V and 9V. Case-2: the void radius is systematically varied, while the void height is kept to be a constant 1 Å. When the radius is increased from 1 Å to 2 Å and 3 Å, the void volume is correspondingly increased from V to 4V and 9V. Fig. 7 shows the calculated ideal strength as a function of the void volume change. It is seen from Fig. 7 that the dimension in the z direction (i.e., in the axial direction) has a smaller effect on the ideal strength than the dimension in the x and y directions (i.e., in the radial direction). Note that the void considered here is a cylinder. For the above two cases, the strain corresponding to the ideal strength (i.e., the critical strain) does not vary with the volume change, remarkably; the critical strain is about 0.14.

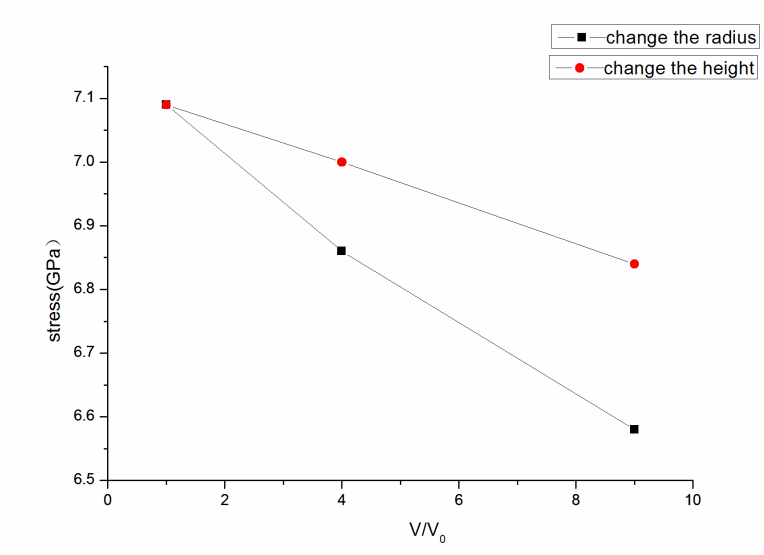

FIG. 7: (Color online) The calculated ideal strength as a function of the void volume change under <100> uniaxial tension.

Now we again use the ATOMEYE software and centro-symmetry parameter to highlight the induced defects during the void growth. A sequence of deformed atomic configurations for a $20\times20\times20$ simulated system with a cylindrical hole is illustrated in Fig. 8(b)–(d). Both the height and the radius of the hole are 1 Å (the corresponding void volume is V).

To clearly see the defect, we make the perfect atoms invisible. Figs. 8(b)–(d) only show atoms in a non-centrosymmetric environment. Because the critical strain is 0.14, Fig. 8(b) is the image before peak stress, and it indicates that the centro-symmetry is near 0 everywhere except for the void surface atoms, and after the peak stress in the stress-strain curves (Fig. 8(c), Fig. 8(d)), local defects start to nucleate from both the top and bottom sides of the cylindrical void. Since the deformed atomic configurations for different void volumes (4V, 9V) are very similar to those for void volume V (Fig. 8), We can conclude that the peak points in the stress-strain curves correspond to the initiation of partial dislocations (i.e., the initiation of plastic deformation) for both crystalline systems with different void volume. For simplicity, we don't draw the deformed atomic configurations for the different void volumes (4V, 9V) in this article. Therefore it can explain a drop in the stress of the stress-strain curves. For perfect crystal Al and single crystal Al with a cylindrical hole (radius and height: 1 Å), the calculated tensile strengths are 11.33 GPa and 7.09 GPa. The introduction of a cylindrical hole (radius and height: 1 Å) leads to about a 37% drop in tensile strength.

III-2-2. Grain boundary effect

A grain boundary is the interface between two grains, or crystallites, in a polycrystalline material. The grain boundary (GB) has great influence on the deformation and fracture of a material. In order to study the effect of a GB, we simulate a symmetric tilt GB $\Sigma 5(310)$. The GB is constructed using the coincidence site lattice (CSL) model [24]. We create the GB model by concatenating two separate grains with specific crystallographic orientations. In-plane translations and atom deletion criteria are used to sample a large number of potential structures to find the global minimum energy GB structure. According to the CSL notation and the GB normal direction, the GB is termed $\Sigma 5(310)$. The GB energy is defined as the minimum energy of GB structures. A nonlinear conjugate gradient algorithm is used for energy minimization. The GB energy is calculated as 567.57 $\mathrm{mJ/m^2}$, which agrees with calculated and experimentally measured energies. After the GB is generated, we proceed with the simulation loops for the GB deformation. First we perform energy minimization of the simulation cell by iteratively adjusting the atom coordinates. Then the simulation cell is pulled in the y-direction, or perpendicular to the boundary interface, to increase the strain, and the strain is increased for a specified number of times in a loop. At the end of a loop, energy minimization of the simulation cell is performed again. And the stress is calculated at each point before the start of a new simulation loop. The maximum tensile stress in the uniaxial extension normal to the interface is about 7.31 GPa at the critical strain 0.166, which is about 65% of the theoretical values 11–12 GPa of the strength of a perfect bulk crystal. By using the ATOMEYE software, the underlying deformation pattern is also studied. It should be noted that a dramatic structural change occurs between Fig. 9(a) and Fig. 9(b) though their strain levels differ only by one loading increment. In fact, the deformation from Fig. 9(a) to Fig. 9(b) corresponds to the crystalline system beginning to break. Note that fracture starts in the GB. We know that aluminum has excellent ductility even at low temperature. But the crystalline system with a GB break at strain ≈ 0.178 in our calculations. It is obvious that the grain boundary

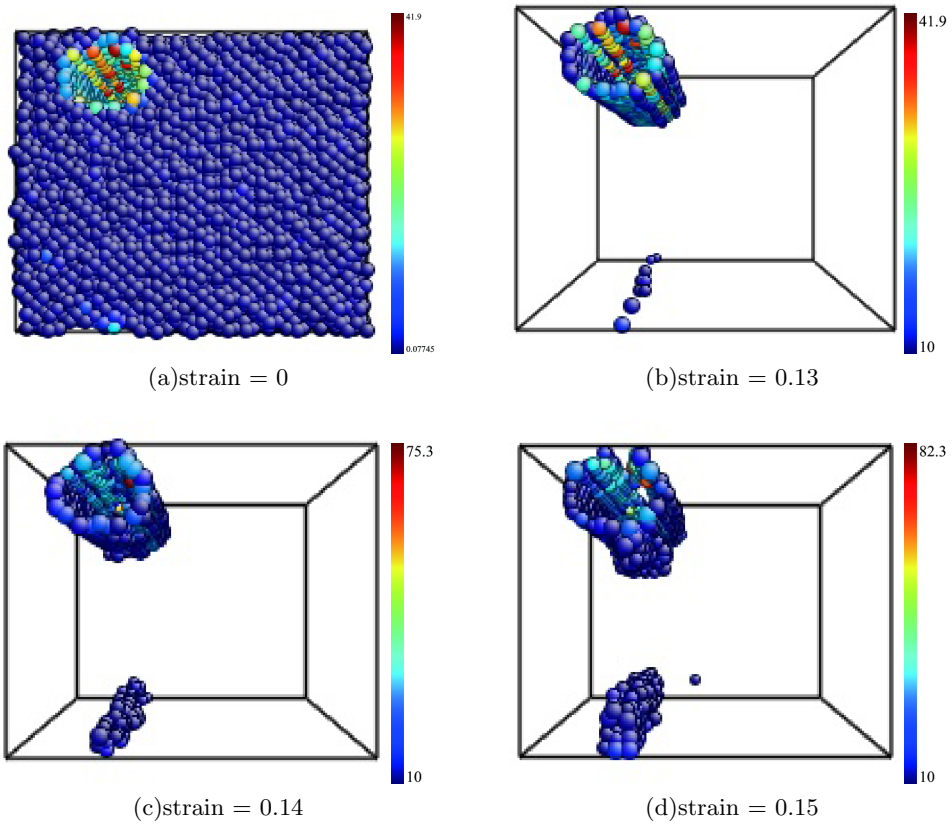

FIG. 8: (Color online) Deformed atomistic configurations for a $20 \times 20 \times 20$ simulated system with a cylindrical hole at 300 K. The height and the radius of the hole are 1 Å. The crystal orientation is [100]-[010]-[001]. The loading is applied along the [100] direction. Atoms are colored according to their central symmetry parameter P in the range between (a) 0 and 41.9, (b) 10 and 41.9, (c) 10 and 75.3, (d) 10 and 82.3.

greatly affects the deformation process.

IV. CONCLUSIONS

In this work, both MD simulations with the EAM potential and first principles calculations have been employed to investigate the uniaxial tension and compression for perfect crystal aluminum. The stress-strain relations generated by MD reproduce the results by first principles in the ideal strengths and the critical strains where the peak stresses appear. MD simulations have been performed to study the cylindrical void effect on the uniaxial tension of Al. The obtained simulations show that the dimension in the axial direction has a smaller effect on the ideal strength than the dimension in the radial direction. A

(a) (b)

FIG. 9: (Color online) Deformed atomistic configurations for a symmetric tilt GB $\Sigma5(310)$ at 300 K. The stress is applied in the y-direction, or perpendicular to the boundary interface. Atoms are colored according to their central symmetry parameter P. (a) strain = 0.177, (b) strain = 0.178 (GB break strain).

defect pattern accompanied with the dislocation nucleation and emission from the void free surface are observed. To study the effect of the GB, we simulate a symmetric tilt GB $\Sigma5(310)$ and strain is imposed perpendicular to the boundary interface. And we can clearly see that fracture starts at the GB. Besides, we can also draw the following conclusion: the temperature, strain rate, and deformation direction have large influences on the value of the ideal strength.

Acknowledgements

We are grateful to Li Peng , Shen Yan-Hong, Gong Yan-Rong, and Ma Jang-Jang for helpful comments and discussion.

References

[1] S. Schumann and H. Friedrich, Mater. Sci. Forum **51**, 419 (2003).
[2] L. Schlapbach and A. Zuttel, Nature **414**, 353 (2001). doi: 10.1038/35104634
[3] B. Smola, I. Stulíková, F. V. Buch, and B. L. Mordike, Mater. Sci. Eng. A **324**, 113 (2002). doi: 10.1038/35104634
[4] A. Kelly and N. H. Macmillan, *Stong solids* 3rd ed. (Clarendon Press, Oxford, 1986) pp 1–56.
[5] J. W. Morris, Jr. C. R. Krenn, D. Roundy, and M. L. Cohen, *Phase Transformations and Evolution in Materials*, eds. P. E. Turchi and A. Gonis (TMS, Warrendate, PA, 2000) pp 187–207.

[6] S. Xu, Y. F. Guo, and A. H. W. Ngan, Int. J. Plasticity. **43**, 116 (2013). doi: 10.1016/j.ijplas.2012.11.002
[7] K. Giles, E. Paul, M. B. Eduardo, R. Bruce, and S. W. Justin, Phys. Rev. B **81**, 092102 (2010). doi: 10.1103/PhysRevB.81.092102
[8] L. Yuan, D. Shan, and B. Guo, J. Mater. Process. Technol. **184**, 1 (2007). doi: 10.1016/j.jmatprotec.2006.10.042
[9] K. J. Zhao, C. Q. Chen, Y. P. Shen, and T. J. Lu, Comput. Mater. Sci. **46**, 749 (2009).
[10] M. I. Albert, V. D. Sergey, and U. Yoshitaka, Phys. Rev. B **84**, 22418 (2001).
[11] D. M. Clatterbuck, C. R. Krenn, L. C. Marvin, and J. W. Morris, Jr., Phys. Rev. Lett. **91**, 135501 (2003). doi: 10.1103/PhysRevLett.91.135501
[12] W. Zhou, Y. Zhang, H. Sun, and C. F. Chen, Phys. Rev. B **86**, 054118 (2012). doi: 10.1103/PhysRevB.86.054118
[13] M. S. Daw and M. I. Baskes, Phys. Rev. B **29**, 6443 (1984). doi: 10.1103/PhysRevB.29.6443
[14] Y. Mishin *et al.*, Phys. Rev. B **59**, 3393 (1999). doi: 10.1103/PhysRevB.59.3393
[15] S. J. Plimpton, J. Comp. Phys. **117**, 1 (1995). doi: 10.1006/jcph.1995.1039
[16] J. Li, Modelling. Simul. Mater. Sci. Eng. **11**, 173 (2003). doi: 10.1088/0965-0393/11/2/305
[17] P. Villars, *Pearson's Handbook of Crystallographic Data for Intermetallic Phases, Desk Edition* (American Society for Metals, Materials Park, OH, 1997).
[18] G. Simmons and H. Wang, *Single Crystal Elastic Constants and Calculated Aggregate Properties: a Handbook*, 2nd ed. (M. I. T. Press, Cambridge, Massachusetts, 1971).
[19] G. Kresse and J. Hafner, Phys. Rev. B **47**, 558 (1993); doi: 10.1103/PhysRevB.47.558G. Kresse and J. Furthmuller, Phys. Rev. B **54**, 11169 (1996). doi: 10.1103/PhysRevB.54.11169
[20] J. P. Perdew *et al.*, Phys. Rev. B **46**, 6671 (1992). doi: 10.1103/PhysRevB.46.6671
[21] P. E. Blochl, Phys. Rev. B **50**, 17953 (1994); doi: 10.1103/PhysRevB.50.17953G. Kresse and D. Joubert, Phys. Rev. B **59**, 1758 (1999). doi: 10.1103/PhysRevB.59.1758
[22] H. J. Monkhorst and J. D. Pack, Phys. Rev. B **13**, 5188 (1976). doi: 10.1103/PhysRevB.13.5188
[23] C. L. Kelchner, S. J. Plimpton, and J. C. Hamilton, Phys. Rev. B **58**, 11085 (1998). doi: 10.1103/PhysRevB.58.11085
[24] S. Ranganathan, Acta. Cryst. **21**, 197 (1966). doi: 10.1107/S0365110X66002615